Polyvalent Mesoporous Silica Nanoparticle-Aptamer Bioconjugates Target Breast Cancer Cells

Le-Le Li, Qian Yin, Jianjun Cheng, and Yi Lu**

This paper is dedicated to the memory of Prof. Victor S.-Y. Lin.

Spatiotemporal control over the delivery of therapeutic agents is an outstanding challenge to cancer treatment. By taking advantage of recent advances in DNA aptamer biology and mesoporous silica nanotechnology, we report a general approach to design and fabricate controlled release drug delivery systems that are able to effectively target cancer cells. Specifically, polyvalent mesoporous silica nanocarriers-aptamer bioconjugates were constructed; the high-surface-area nanoporous core allowed high drug loading and the surface-conjugated aptamer facilitated the nanoparticle targeting of nucleolin overexpressed MCF-7 cells. The efficient cancer-cell-specific fluorescent imaging and drug delivery of the bioconjugates outline the great potential for therapeutic applications.

1. Introduction

Targeted drug delivery mediated by multivalent nanomedicines is expected to change the landscape of oncology as it allows a high therapeutic dose to be delivered to the target site and mitigate undesired side effects of conventional chemotherapy.[1] In the past few years, mesoporous silica nanoparticle (MSN) has emerged as a promising nanomedicine platform because of its excellent biocompatibility, tailorable pore size with a diameter of 2–50 nm allowing for the storage and controlled release of sensing, imaging or therapeutic agents, considerable surface areas and large pore volume for loading of cargos with high efficiency, and tunable particle size between 50 and 150 nm for efficient cellular uptake and trafficking.[2] There has been tremendous interest of developing smart MSN nanocarriers that are able to respond to either external (e.g., light and magnetic field) or internal stimuli (e.g., redox, enzymes and pH).[3] Most recently, surface-functionalized MSNs were also used for selectively targeting of malignant cells using cancer-specific agents.[4] The combination of well-established knowledge from mesoporous materials with the current experience in biotechnology will be an important step in realizing the full potentials of MSNs as theranostic nanomedicines.[1,4]

Aptamers, single-stranded oligonucleotides that can bind a wide array of biological targets with high affinity and specificity comparable to those of antibodies,[5,6] emerged as new targeting moieties for therapeutic applications. They are obtained through a combinatorial biology technique called systematic evolution of ligands by exponential enrichment (SELEX). Being nonimmunogenic, DNA aptamers offer distinct advantages over antibodies as convenient and evolvable targeting groups for drug delivery because of their smaller size, higher ratio of target accumulation, easier production without the use of animal, and higher in vivo stability.[7] However, the polyanionic nature of the aptamers makes it difficult for penetrating through the cell membranes. This limitation can be overcome by functionalizing the aptamers onto nanocarriers. Aptamer has been actively used to functionalize polymeric nanoparticles with various compositions, structures, and porosities to realize targeted drug delivery and diagnostic imaging.[1a,8] Recently, DNA-functionalized inorganic nanoparticles have also been used for drug delivery.[9,10] Since such used inorganic nanoparticles are non-porous, drugs have to be attached to the surface and the drug loading capacity was limited.[10] Herein, we introduce the cancer-specific aptamer into MSN-based nanocarriers to construct an efficient imaging and targeting drug delivery platform with several attractive features (**Figure 1**a): (1) due to the outstanding characteristics of porosity and biocompatibility, MSNs core are able to incorporate various drugs into the mesopores; (2) their silanol-containing surface can be easily functionalized to control the drug release; (3) multiple aptamers on external surface of MSNs resulted in multivalent effect for an enhanced specific binding and cell uptake; (4) complementary DNA (cDNA) could reversibly regulate cell targeting of MSN-aptamer bioconjugates.

Dr. L. Li,[†] Prof. Y. Lu
Department of Chemistry
University of Illinois at Urbana-Champaign
Urbana, IL 61801, USA
E-mail: yi-lu@illinois.edu
Q. Yin,[†] Prof. J. Cheng
Department of Materials Science and Engineering
University of Illinois at Urbana-Champaign
Urbana, IL 61801, USA
E-mail: jianjunc@illinois.edu
[†] These authors contributed equally to this work

DOI: 10.1002/adhm.201200116

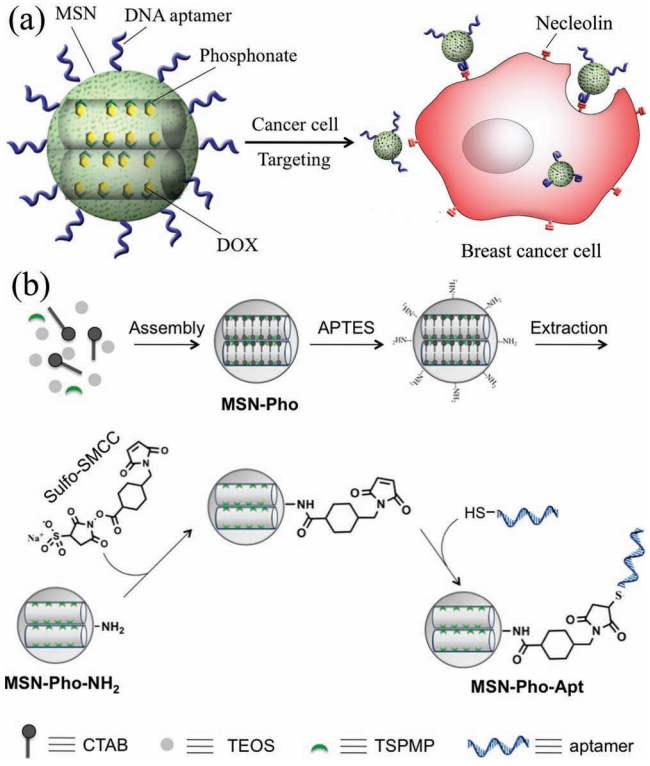

Figure 1. (a) Schematic illustration of the structure of the polyvalent nucleic acid aptamer functionalized mesoporous nanocarriers and the targeted delivery of doxorubicin to breast cancer cells. (b) Schematic illustration of the preparation procedure of the targeted delivery system.

2. Results and Discussion

2.1. Design, Synthesis and Characterization of Mesoporous Silica Nanoparticle-Aptamer Bioconjugates

To obtain aptamer-functionalized MSN nanocarriers for cancer-specific drug delivery, we designed a synthetic scheme of co-condensation of phosphonate groups into the internal channels of MSNs, modification of the surface of resulting MSN-Pho with a amine group and subsequent post-grafting of a thiolated DNA aptamer onto the external MSN surface (Figure 1b). The internal mesopores was modified with phosphonate groups in order to load positively charged doxorubicin (DOX) drug molecules through a proton-sensitive electrostatic binding interaction.[11] The MSNs modified with phosphonate groups (MSN-Pho) were first synthe-sized by following a base-catalyzed co-condensation procedure, which allow for a homogeneous distribution of organic groups on the pore surface.[3a] The resulting MSN-Pho that contains MCM-41-type channel-like mesoporous structure was confirmed by TEM images and X-ray diffraction (Figure S1 and S2, respectively). The N_2 adsorption–desorption isotherms of MSN-Pho further revealed a type IV curve with a specific surface area of 1040 m^2/g and an average pore diameter of 2 nm (Figure S3).

To provide cancer-targeting capability to MSNs, we chose a 26-mer DNA aptamer AS1411, the first aptamer to enter clinical oncology trials with promising antitumor activity and minimal systemic toxicity.[12] The AS1411 has been shown to be highly specific to interact with nucleolin (NCL),[13] a protein that is overexpressed on the plasma membrane of several types of cancer cells, including breast cancer cells such as MCF-7 and MDA-MB-231.[14] The sequence of the aptamer used in this study (5 -GGT GGT GGT GGT TGT GGT GGT GGT GGT TTT TTT TTT-thiol-3, called the NCL-aptamer) contains ten extra T bases at the 3 -terminus to ensure that the binding domains of the aptamer extended away from silica surface to minimize non-specific interactions with MSN while maximizing specific targeting of cancer cells. In addition, the NCL-aptamer contains a thiol group at the 3 -end to allow conjugation to the MSNs.

To functionalize the MSN-Pho with NCL-aptamer, the external surface of as-synthesized MSN-Pho was first modified with amine groups through reacting with 3-aminopropyltriethoxysilane (APTES). The grafted APTES on MSNs was estimated to be 1.1 mmol/g SiO_2 based on elemental analysis. The resulting MSN-Pho-NH_2 was reacted with a bifunctional cross-linker sulfosuccinimidyl-4-(N-maleimidomethyl) cyclohexane-1-carboxylate (Sulfo-SMCC) which contains an amine-reactive N-hydroxysuccinimide functional group (NHS ester) and a sulfhydryl (thiol)-reactive maleimide group. The maleimide-terminated MSNs were subsequently conjugated with the 3 -thiol-modified DNA aptamer to produce MSN-Pho-Apt, which was confirmed by the decrease of typical absorbance of DNA at 260 nm in the supernatant after the conjugation (Figure S4). The control experiment showed that the cleavage of DNA aptamer by TCEP to obtain free sulfhydryl groups was the key step for modification of maleimide-functionalized MSNs through the sulfhydryl-maleimide coupling reaction. This experiment further confirmed that the aptamer was attached to the MSNs through covalent bond but not via nonspecific interactions (Figure S4). The amount of immobilization was determined to be 1.5 mol/g SiO_2 based on UV/Vis spectroscopy. The successful conjugation of the NCL-aptamer onto MSNs was also confirmed by the appearance of the characteristic asymmetric stretching mode of the imidyl group (1710 cm^{1}) and the amide vibrations (1550 cm^{1}) in the FTIR spectroscopy (Figure S5).

The TEM image of the resulting MSN-Pho-Apt shows that it retained highly ordered mesoporous structure with particle diameters of about 140 nm (**Figure 2**a). Zeta potential measurements (Figure 2b) showed that MSN-Pho nanoparticles were highly negatively charged (–38.1 mV) and became slightly positively charged (10.1 mV) after amine modification. The nanoparticles became highly negatively charged again after their surface was conjugated with DNA aptamers (–38.5 mV). To test the functionality of the DNA aptamer on the MSNs, the MSN-Pho-Apt were incubated with 5-nm gold nanoparticles (AuNPs) that were modified with thiolated complementary DNA (cDNA). As shown inFigure 2c, MSN-Pho-Apt was surrounded by a number of AuNPs, forming the satellite-like nanostructure. As a comparison, the assembly of the nanoparticles was not observed when AuNPs was functionalized with non-complementary DNA (Figure 2d). These results indicated that DNA molecules were not only covalently functionalized to MSN-Pho-Apt in a large number but also retained their specific hybridization property to targets. The drug loading was accomplished by soaking MSN-Pho-Apt in a solution of 3.4 mM DOX to allow the drug molecules to diffuse into the pores. The loading percentage by weight of DOX in MSN-Pho-Apt was found to be 4.6%. Next, we investigated the in vitro drug release kinetics of the DOX loaded MSN-Pho-Apt

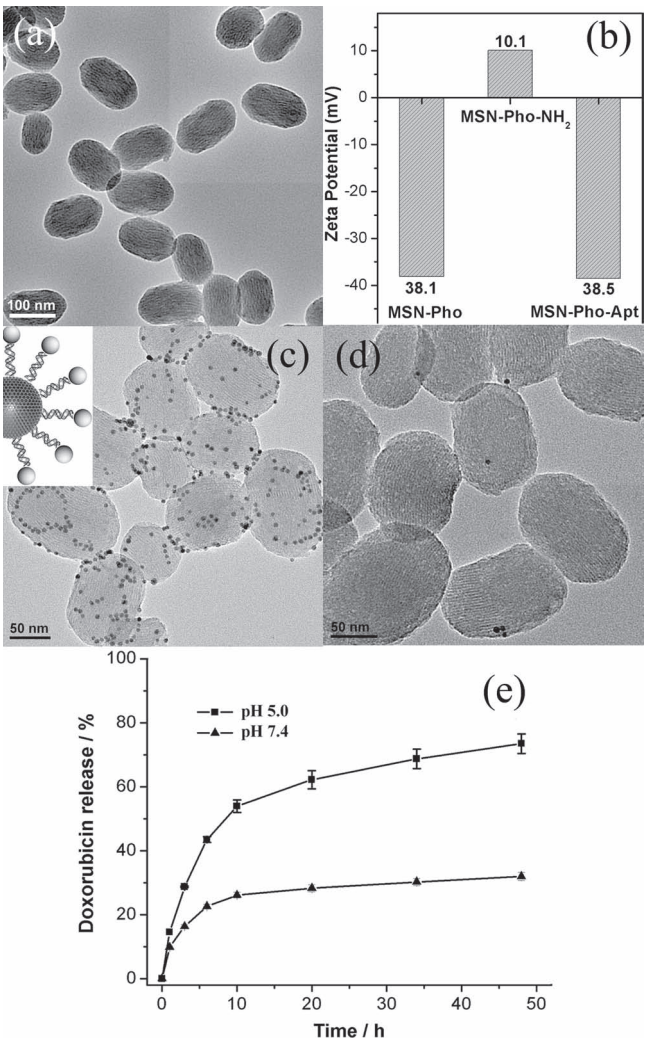

Figure 2. (a) TEM micrograph of the nanocarrier MSN-Pho-Apt. (b) Zeta potential of MSN-Pho, MSN-Pho-NH_2, and MSN-Pho-Apt. TEM images of MSN-Pho-Apt after assembly with 5 nm AuNPs that was functionalized with (c) cDNA and (d) non-complementary DNA. (e) The time-dependent release profile of DOX from drug loaded MSN-Pho-Apt in phenol-red-free DMEM with different pHs.

in cell growth medias at pH 5.0 and 7.4 (Figure 2e). As expected, the drug release rate was pH-dependent, displaying increased release kinetics at increased acidities. The phosphonate group on the surface of mesopores was protonated with decreased pH so that the electrostatic interaction between the carriers and DOX was weakened, leading to more DOX released.[11] Given the known high acidity in the tumor interstitium and in the cellular endosomes, such pH-responsive drug release in our system provides an additional benefit in cancer therapy.

2.2. Targeting Breast Cancer Cells and Anticancer Efficacy

To test the targeting specificity of the nanocarriers, fluorescein attached mesoporous silica nanoparticle was prepared by similar co-condensation method. The resulting MSN-FITC was used for the DNA functionalization, and then incubated separately with MCF-7 cells (NCL+) at 37 C for 4h. Subsequent analysis using confocal microscopy (**Figure 3**a) revealed that samples exposed to MSN-FITC bearing NCL-aptamer (MSN-FITC-Apt) showed excellent binding and internalization of MSN-FITC-Apt into the MCF-7 cells. The fluorescence was observed predominantly in the cytoplasm of MCF-7 cells instead of nucleus, which was consistent with the projected receptor-mediated endocytosis mechanism. In comparison, the MSN-FITC with no exterior modification and the MSN-FITC modified with a control DNA of a randomized sequence (MSN-FITC-Rdm) showed minimum uptake of the MCF-7 cells, confirming the role of the specific aptamer sequence in cell targeting. To validate that the targeting was indeed mediated by NCL-aptamer, we performed similar experiments in the LNCaP cells (NCL-). MSN-FITC-Apt exhibited drastic difference with respect to their capability of being internalized to LNCaP and MCF-7 cells (Figure S6), indicating that the aptamer-modified nanocarriers have negligible binding affinity with non-targeted cells.

For effective application of pH-responsive MSN-aptamer bioconjugates as targeted imaging and drug delivery system, it is necessary to verify the intracellular location of the nanoparticles. This objective was accomplished by incubating the MSN-FITC-Apt with MCF-7 cells, followed by staining the lysosomal compartments with red fluorescent lysotracker. Imaging of the cells demonstrated the green fluorescence of MSN-FITC-Apt was co-localized with lysotracker red fluorescence (Figure 3b), indicating that the MSN-FITC-Apt resided in the endolysosomal compartments.

Since one unique feature of aptamers is that their activity can be inhibited by their complementary DNAs (cDNAs), we explored whether we could use the cDNA of the NCL aptamer to actively regulate cell targeting of MSN-aptamer bioconjugates. We conducted experiments in which MSN-FITC-Apt nanoparticles were incubated with MCF-7 cells in media containing cDNA (0 and 5 equiv relative to the NCL-aptamer). Subsequent analysis using confocal microscopy revealed that MSN-FITC-Apt co-incubated with cDNA showed substantially reduced uptake of the MCF-7 cells (Figure 3c), indicating that cDNA effectively blocked MSN-FITC-Apt delivery into the cells. The cDNA-induced inhibition of NP uptake is because the complementary base pairing disrupts G-quadruplex structure of NCL-aptamer that is critical for the binding to NCL receptors. Therefore, the cDNA of the targeting aptamer can function as an antidote to deactivate the NCL-aptamer on MSNs and inhibit its cellular uptake, which can be extremely useful for reversing the undesired toxicity in the case of drug overdose.

To verify that MSN-FITC-Apt was indeed internalized and the fluorescence was not simply due to the surface bound MSN-FITC, we conducted further analysis using flow cytometry. MCF-7 cells were similarly treated with MSN-FITC-Apt except that, before formaldehyde fixing, 0.25% trypsin, a common protease, was added to break down any cell surface proteins. This step ensured that no membrane nucleolins were available to bind to MSN-FITC-Apt. Therefore, the fluorescence activities were from the MSN-FITC-Apt nanocarriers which were internalized into the cells. The nanocarriers treated and untreated cells were then analyzed in a flow cytometer to measure fluorescence intensity from each individual cell. The histograms

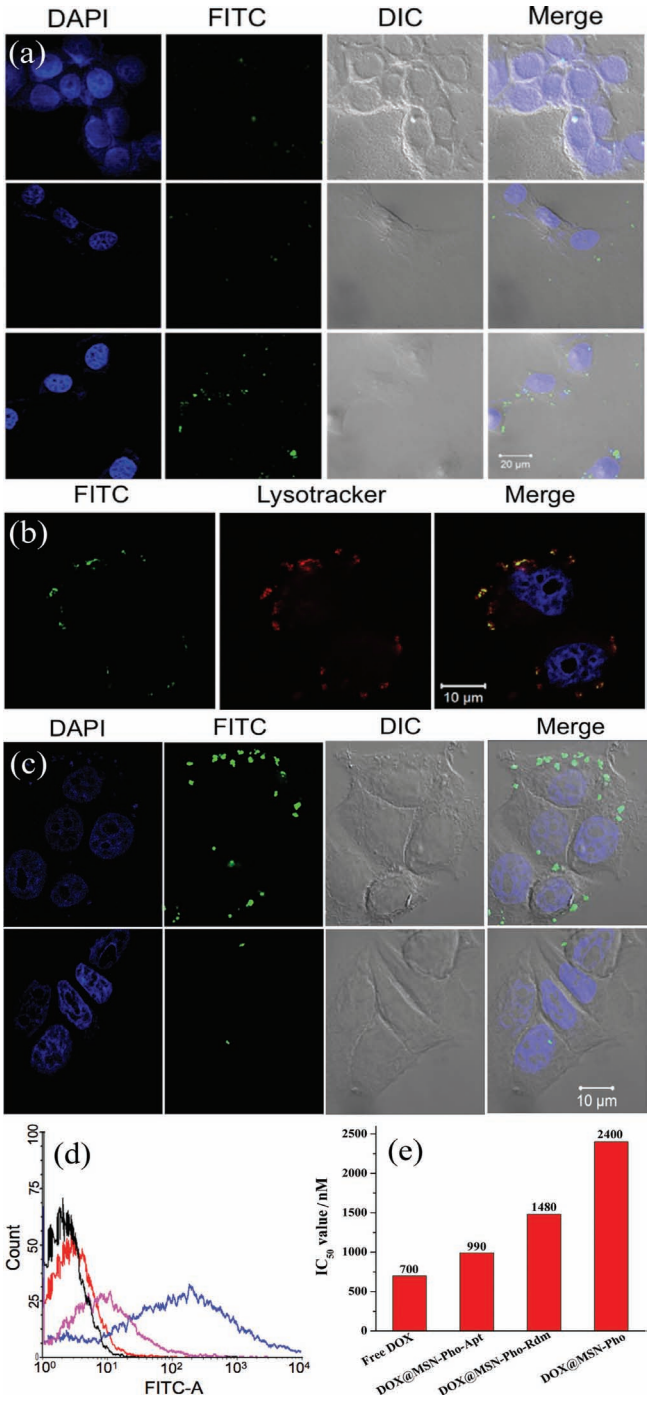

Figure 3. (a) Confocal Microscopy images of MCF-7 cells treated with MSN-FITC (upper), MSN-FITC-Rdm (middle) and MSN-FITC-Apt (lower). (b) Confocal microscopy images showing MSN-FITC-Apt uptake into the MCF-7 cells that was labeled with lysotracker to mark lysosomes (red). (c) Confocal microscopy images of MCF-7 cells treated with MSN-FITC-Apt in media containing cDNA of 0 (upper) and 5 (lower) equiv relative to the NCL-aptamer. (d) Flow cytometry analysis of untreated MCF-7 cells (black line); MCF-7 cells treated with MSN-FITC (red line), MSN-FITC-Rdm (purple line) and MSN-FITC-Apt (blue line). (e) MTT assay of free DOX, DOX-loaded MSN-Pho (DOX@MSN-Pho), DOX-loaded MSN-Pho-Rdm (DOX@MSN-Pho-Rdm), and DOX-loaded MSN-Pho-Apt (DOX@MSN-Pho-Apt) in MCF-7 cells.

showing numbers of cells exhibiting different fluorescence intensity (Figure 3d) indicates a clear shift to higher fluorescence on the MCF-7 cells treated with MSN-FITC-Apt in comparison with the untreated MCF-7 cells, the cells treated with MSN-FITC and MSN-FITC-Rdm. MSN-FITC-Rdm displayed a slight increase in fluorescence compared to the untreated ones and the cells treated with MSN-FITC only, which illustrated the non-specific interaction of DNA to the cells. This is consistent with what was reported by Mirkin and coworkers, who recently demonstrated that the DNA-nanoparticle conjugates exhibit significantly high cellular uptake due to the binding between negatively charged DNA with positively charged trafficking proteins in the cell membrane.[9,15] These experiments confirmed that the aptamer-functionalized MSNs can selectively bind to NCL on the surface of MCF-7 breast cancer cells and are internalized via receptor-mediated endocytosis.

We used the MTT assay to evaluate the anti-cancer activity of DOX-loaded MSN-Pho-Apt in MCF-7 cell. The NCL aptamer has low cytotoxicity towards MCF-7 cells; MCF-7 cells treated with MSN-Apt alone without DOX showed negligible cell death even at the concentration of 1 mg/mL (Figure S8), indicating excellent biocompatibility of MSN-Apt and that the quantity of aptamers used here was unable to induce cell toxicity. In contrast, a considerable increase in the antitumor activity was observed in aptamer-conjugated DOX-loaded MSN-Pho-Apta (IC_{50} = 990 nM,Figure 3e), which is substantially more toxic than the DOX-loaded MSN-Pho-Rdm (IC_{50} = 1.5 M) and DOX-loaded MSN-Pho with no exterior modification (IC_{50} = 2.4 M). These experiments showed that successful implementation of combing cell-recognizing aptamers with MSNs to effectively deliver DOX to diseased cells to maximize its therapeutic efficacy and minimize its side effects.

3. Conclusion

In conclusion, we have integrated cancer-targeting DNA aptamer with mesoporous silica particles to create a general platform for the design and fabrication of selective imaging and targeted drug delivery system. The NCL aptamer was conjugated to the external MSN surface for targeting breast cancer cells, while the drug molecules encapsulated inside the nanopores showed pH-dependent controlled release kinetics. The aptamer-facilitated reversibly cellular uptake of the resulting nanocarriers into MCF-7 cells via receptor-mediated endocytosis was demonstrated, outperforming the non-targeting nanoparticles. Since aptamers specific for a variety of molecular markers and metabolites in the biological systems can be obtained through SELEX, this novel targeting strategy in conjugation with the MSN drug delivery system can be potentially applied to many other imaging and delivery systems capable of specifically binding to various target cells and delivering high doses of other therapeutics.

4. Experimental Section

Materials: Tetraethylorthosilicate (TEOS), N-cetyltrimethylammonium bromide (CTAB), 3-aminopropyltriethoxysilane (APTES), 3-Trihydroxysilylpropyl methylphosphonate (TSPMP), fluorescein isothiocyanate (FITC, 90%), doxorubicin hydrochloride (Dox, 98%) were purchased from Sigma-Aldrich. Sulfosuccinimidyl 4-[N-maleimidomethyl]

cyclohexane-1-carboxylate (Sulfo-SMCC) and tris(2-carboxyethyl) phosphine hydrochloride (TCEP) were from Thermo Scientific. Dulbecco's modified eagle's medium (DMEM) was purchased from Invitrogen (Carlsbad, CA). MCF-7 (used for MTT assays) and LNCaP cells (used for cellular internalization studies) were purchased from ATCC (Manassas, VA, USA) and cultured in DMEM medium and RPMI medium 1640 containing 10% FBS (Fetal Bovine Serum), 1000 units/mL aqueous Penicillin G and 100 g/mL streptomycin. AuNPs (5 nm diameter) were purchased from Ted Pella, Inc. (Redding, CA). The thiolated DNA were synthesized and purified by Integrated DNA Technologies, Inc. (IDT, Coralville, IA). The sequences are as follows:

NCL-aptamer: 5 -GGT GGT GGT GGT TGT GGT GGT GGT GGT TTT TTT TTT-thiol-3

Random DNA: 5 -GAG AAC CTG AGT CAG TAT TGC GGA GAT TTT TTT TTT-thiol-3

cDNA for AuNPs functionalization: 5 -ACA ACC ACC ACC ACC TTT TTT TTT-thiol-3

Noncomplementary DNA for AuNPs functionalization: 5 -GGT GGT GGT GGT TGT TTT TTT TTT-thiol-3

cDNA for regulation of cell targeting: 5 -CCA CCA CAA CCA CCA CCA CC-3

Preparation of MSNs and subsequent post-modification: Briefly, CTAB (1 g) and NaOH (aq) (3.50 mL, 2.00 M) were added in distilled water (480 mL), followed by adjusting the solution temperature to 80 C. TEOS (5.00 mL) and 3-Trihydroxysilylpropyl methylphosphonate (TSPMP, 0.6 mL) were then added slowly to the solution. The mixture was allowed to stir for 2 h at 80 C to give rise to precipitates. The solid product was filtered, washed with deionized water and methanol, and dried in vacuum to yield the as-synthesized MSN-Pho. The surfactant templates (CTAB) were then removed from the pores by refluxing in acidic methanol. The attachment of amino group to the particle surface was obtained based on the reaction of the MSN-Pho with 3-aminopropyl trimethoxysilane (APTS) in dry toluene. As for fluorescein-labeled mesoporous silica nanoparticles (MSN-FITC), fluorescein isothiocyanate (FITC, 2 mg) was first reacted with APTES (44 L) in ethanol (1 mL) for 2h in the dark, and then it was added with TEOS to the surfactant solution.

DNA aptamer conjugation: A bifunctional cross-linker Sulfo-SMCC was used to functionalize MSN with DNA aptamer. MSN-Pho-NH_2 (10 mg) was well suspended in a mixture solution of PBS buffer (100 mM PBS, 150 mM NaCl, pH 7.3) and DMF (7:3) containing excess Sulfo-SMCC (4 mg) for several hours. The resulting particles were collected by centrifugation, extensively washed with DMF and PBS buffer and give rise to maleimide-modified MSN-Pho. Further functionalization of the DNA aptamer was performed by first incubating 20 nmol of DNA with three equivalent of TCEP to obtain free sulfhydryl groups. Then, the purified DNA was mixed with maleimide-modified MSN-Pho in conjugation buffer (100 mM PBS, 1 M NaCl, pH 7.3) and shaken at room temperature for 24 h. The particle was recovered by centrifugation and washing with the conjugation buffer. All the supernatant was collected for UV/Vis absorbance measurement. The immobilization efficiency of 1.5 mol/g SiO_2 was determined based on the absorbance difference at 260 nm between the DNA solution before and after immobilization.

Synthesis of DNA functionalized 5 nm AuNPs and its assembly with aptamer conjugated MSNs: Thiol-modified DNA were chemically attached to the AuNPs (5 nm) according to our previously reported method.[16] Thiol-modified DNA molecules were first activated by 1.5 equiv of TCEP for 1 h under pH 5.2 at room temperature before use. Glass vials (20-mL volume) were soaked in 12 M NaOH for 1 h and rinsed with DI water before use. AuNPs were loaded into the NaOH-treated glass vials, and thiol-modified DNA was added to a final concentration of 3 M. The vials were capped and kept at room temperature for about 16 h. Tris acetate buffer (pH 8.2) was then added to the nanoparticles to a final concentration of 5 mM, and NaCl was added to a final concentration of 100 mM. The functionalized 5 nm AuNPs solutions were incubated for another day before usage. To purify the product, microcon (Ultracel YM-100, MWCO = 100K, Microcon) was used by following the instructions from the manufacturer. The DNA aptamer conjugated MSNs were incubated with cDNA or noncomplementary DNA functionalized 5 nm AuNPs in Tris-HCl buffer (20 mM, 100 mM NaCl, 2 mM KCl, 1 mM $MgCl_2$, pH7.4) over night. The nanoparticles were then centrifuged and washed to remove unassembled AuNPs.

Drug loading and in vitro release experiments: The nanocarriers (10 mg) were incubated in DOX solution (0.5 mL, 3.4 mM) for 12 h. The DOX-loaded nanocarriers were then centrifuged and washed with water. All the washing solutions were collected and the loading of DOX was calculated from the difference of the DOX concentrations in the initial and collected solution. To test the pH-dependent drug release properties, DOX-loaded nanocarriers were dispersed into phenol red-free DMEM medium (pH 7.4 or acidified to pH 5.0). The supernatants were taken from the suspension at a give time interval and cleared by centrifugation for monitoring the release of the drug via the fluorescence of DOX.

Analysis of cellular uptake by fluorescence microscope and flow cytometry: MCF-7 and LNCaP cells were grown in chamber slides in Dulbecco's modified Eagle's medium (DMEM) and RPMI medium 1640 (American Type Culture Collection), respectively, supplemented with aqueous penicillin G (100 units/ml), streptomycin (100 g/mL), and FBS (10%) at concentrations to allow 70% confluence in 24 h (i.e., 40,000 cells per cm^2). On the day of experiments, the medium was removed and washed with prewarmed PBS (500 L for each chamber), and then incubated with prewarmed Opti-MEM medium (phenol red reduced) for 30 min before the addition of the MSN-based nanocarriers. The cells were co-incubated with MSN-based nanocarriers for 4 h and then washed with PBS (3 500 L), fixed with 4% formaldehyde, and subsequently imaged on a Scanning Confocal Microscope. Nucleuses were stained by DAPI. Control samples without nanoparticle addition were also imaged. For the analysis with flow cytometry, there were 10 000 cells measured in each sample. Both percentage of fluorescence positive cells (We assume that 0.5% of untreated cells were positive, so we can set up a gate for fluorescence positive cells when analyzing FACS data) and mean fluorescence were quantified. Each sample was measured in triplicate.

Cytotoxicity of DOX-loaded nanocarriers: MCF-7 cells were placed in a 96-well plate for 24 h (10 000 cells per well). On the experimental day, cells were washed with 100 L of prewarmed PBS. Freshly prepared DOX-loaded nanocarriers (prepared in 1 PBS, 100 L) were added to the cell. The cells were incubated for 6 hours and then washed with PBS (3 100 L). Free DOX was used as a positive control. Untreated cells were used as a negative control. The cells were further incubated in pre-warmed growth medium for 72 h in a 5% CO_2 incubator at 37 C. The standard MTT assay protocols were followed thereafter.

Instrumentation: Transmission electron microscopy (TEM) images were taken on the JEOL 2100 Cryo transmission electron microscope with an accelerating voltage of 200 kV. X-ray powder diffraction patterns were recorded using Cu K (= 1.5418) radiation with a Seimens-Bruker D5000 instrument operating at 40 kV and 30 mA. Fourier-transform infrared spectra (FTIR) spectra were recorded on a Mattson Infinity Gold FTIR spectrometer. The nitrogen adsorption and desorption isotherms were measured at 77 K using a Micromeretics ASAP 2010 instrument. Zeta potential was measured on a Malvern Zetasizer 3000 (Malvern Instruments). UV/Vis spectra were recorded on a Hewlett–Packard 8453 spectrometer. Fluorescent spectra were recorded on a FluoroMax-P fluorimeter (HORIBA Jobin Yvon Inc., Edison, NJ). Absorbance at 590 nm was read by microplate reader (Perkin Elmer, Victor$^3{}_{TM}$ V) for MTT assay. Confocal microscopy images for cell internalization studies were taken by Zeiss LSM 700 Laser Scanning Confocal Microscope using a 63X oil lens and excitation wavelength set at 488 nm. Flow cytometry analysis was conducted with a BD FACSCanto 6 color flow cytometry analyzer (BD, 1 Becton Drive, Franklin Lakes, New Jersey, USA).

Supporting Information

Supporting Information is available from the Wiley Online Library or from the author.

Acknowledgements

This work was supported by the Beckman Institute of the University of Illinois through a Seed Grant, and the US National Science Foundation (CMMI 0749028 and DMR-0117792 to YL) and National Institute of Health (NIH Director's New Innovator Award 1DP2OD007246 and R21 grant 1R21CA152627 to JC).

Received: April 8, 2012
Published online: June 6, 2012

[1] a) S. Dhar, F. X. Gu, R. Langer, O. C. Farokhzad, S. J. Lippard, *Proc. Natl. Acad. Sci.* **2008**, *105*, 17356–17361; b) D. Peer, J. M. Karp, S. Hong, O. C. Farokhzad, R. Margalit, R. Langer, *Nat. Nanotech.* **2007**, *2*, 751–760; c) J. D. Rocca, D. Liu, W. Lin, *Acc. Chem. Res.* **2011**, *44*, 957–968;d) E. J. Kwon, J. Lasiene, B. Jacobson, I. K. Park, P. J. Horner, S. H. Pun, *Biomaterials* **2010**, *31*, 2417–2424; e)Z. Xue, M. Lin, J. Zhu, J. Zhang, Y. Li, Z. Guo, *Chem. Commun.* **2010**, *46*, 1212–1214; f) Y. Wang, P. Brown, Y. Xia, *Nat. Mater.* **2011**, *10*, 482–483; g) M. R. Mozafari, *Nanomaterials and Nanosystems for Biomedical Applications*, Springer, Netherlands **2007**.

[2] a) I. Slowing, J. Vivero-Escoto, C.-W. Wu, V. S.-Y. Lin, *Adv. Drug Delivery Rev.* **2008**, *60*, 1278–1288; b) J. Lu, M. Liong, J. I. Zink, F. Tamanoi, *Small* **2007**, *3*, 1341–1346; c) M. Vallet-Regí, F. Balas, D. Arcos, *Angew. Chem., Int. Ed.* **2007**, *46*, 7548–7558; d) K. M. L. Taylor, J. S. Kim, W. J. Rieter, H. An, W. Lin, W. Lin, *J. Am. Chem. Soc.* **2008**, *130*, 2154–2155; e)J. E. Lee, N. Lee, T. Kim, J. Kim, T. Hyeon, *Acc. Chem. Res.* **2011**, *44*, 893–902; f) J. Liu, A. Stace-Naughton, X. Jiang, C. J. Brinker, *J. Am. Chem. Soc.* **2009**, *131*, 1354–1355.

[3] a) B. G. Trewyn, I. I. Slowing, S. Giri, H.-T. Chen, V. S.-Y. Lin, *Acc. Chem. Res.* **2007**, *40*, 846–853; b)M. W. Ambrogio, C. R. Thomas, Y.-L. Zhao, J. I. Zink, J. F. Stoddart, *Acc. Chem. Res.* **2011**, *44*, 903–913; c) R. Casasús, E. Climent, M. D. Marcos, R. Martínez-Máñez, F. Sancenón, J. Soto, P. Amorós, J. Cano, E. Ruiz, *J. Am. Chem. Soc.* **2008**, *130*, 1903–1917; d) I. I. Slowing, J. L. Vivero-Escoto, B. G. Trewyn, V. S.-Y. Lin, *J. Mater. Chem.* **2010**, *20*, 7924–7937; e) C.-L. Zhu, C.-H. Lu, X.-Y. Song, H.-H. Yang, X.-R. Wang, *J. Am. Chem. Soc.* **2011**, *133*, 1278–1281; f) A. Schlossbauer, J. Kecht, T. Bein, *Angew. Chem., Int. Ed.* **2009**, *48*, 3092–3095; g) H. P. Rim, K. H. Min, H. J. Lee, S. Y. Jeong, S. C. Lee, *Angew. Chem., Int. Ed.* **2011**, *50*, 8853–8857.

[4] a) C. E. Ashley, E. C. Carnes, G. K. Phillips, D. Padilla, P. N. Durfee, P. A. Brown, T. N. Hanna, J. Liu, B. Phillips, M. B. Carter, N. J. Carroll, X. Jiang, D. R. Dunphy, C. L. Willman, D. N. Petsev, D. G. Evans, A. N. Parikh, B. Chackerian, W. Wharton, D. S. Peabody, C. J. Brinker, *Nat. Mater.* **2011**, *10*, 389–397; b) J. D. Rocca, R. C. Huxford, E. Comstock-Duggan, W. Lin, *Angew. Chem., Int. Ed.* **2011**, *50*, 10330–10334; c) Z. Luo, K. Cai, Y. Hu, L. Zhao, P. Liu, L. Duan, W. Yang, *Angew. Chem., Int. Ed.* **2011**, *50*, 640–643; d) M. Liong, J. Lu, M. Kovochich, T. Xia, S. G. Ruehm, A. E. Nel, F. Tamanoi, J. I. Zink, *ACS Nano* **2008**, *2*, 889–896; e) J. M. Rosenholm, E. Peuhu, J. E. Eriksson, C. Sahlgren, M. Lindén, *Nano Lett.* **2009**, *9*, 3308–3311; f) J. Lu, M. Liong, Z. Li, J. I. Zink, F. Tamanoi, *Small* **2010**, *6*, 1794–1805; g) S. Cheng, C. Lee, M. Chen, J. S. Souris, F. Tseng, C. Yang, C. Mou, C. Chen, L. Lo, *J. Mater. Chem.* **2010**, *20*, 6149-6157; h) C. Zhu, X. Song, W. Zhou, H. Yang, Y. Wen, X. Wang, *J. Mater. Chem.* **2009**, *19*, 7765-7770; i) V. Mamaeva, J. M. Rosenholm, L. T. Bate-Eya, L. Bergman, E. Peuhu, A. Duchanoy, L. E. Fortelius, S. Landor, D. M. Toivola, M. Lindén, C. Sahlgren, *Mol. Ther.* **2011**, *19*, 1538-1546; j) C. Tsai, C. Chen, Y. Hung, F. Chang, C. Mou, *J. Mater. Chem.* **2009**, *19*, 5737-5743.

[5] a) A. D. Ellington, J. W. Szostak, *Nature* **1990**, *346*, 818–822; b) C. Tuerk, L. Gold, *Science* **1990**, *249*, 505–510.

[6] a) Y. Lu, J. Liu, *Acc. Chem. Res.* **2007**, *40*, 315–323; b) J. Liu, Z. Cao, Y. Lu, *Chem. Rev.* **2009**, *109*, 1948–1998; c) Z. Wang, Y. Lu, *J. Mater. Chem.* **2009**, *19*, 1788–1798; d) J. H. Lee, M. V. Yigit, D. Mazumdar, Y. Lu, *Adv. Drug Delivery Rev.* **2010**, *62*, 592–605; e) H. Xing, N.-Y. Wong, Y. Xiang, Y. Lu, *Curr. Opin. Chem. Biol.* **2012**, http://dx.doi.org/10.1016/j.cbpa.2012.03.016.

[7] a) K. S. Schmidt, S. Borkowski, J. Kurreck, A. W. Stephens, R. Bald, M. Hecht, M. Friebe, L. Dinkelborg, V. A. Erdmann, *Nucleic Acids Res.* **2004**, *32*, 5757–5765; b) Y. Wu, K. Sefah, H. Liu, R. Wang, W. Tan, *Proc. Natl. Acad. Sci.* **2010**, *107*, 5–10.

[8] F. Gu, L. Zhang, B. A. Teply, N. Mann, A. Wang, A. F. Radovic-Moreno, R. Langer, O. C. Farokhzad, *Proc. Natl. Acad. Sci.* **2008**, *105*, 2586–2591.

[9] N. L. Rosi, D. A Giljohann, C. S. Thaxton, A. K. R. Lytton-Jean, M. S. Han, C. A. Mirkin, *Science* **2006**, *312*, 1027–1030.

[10] a) S. Dhar, W. L. Daniel, D. A. Giljohann, C. A. Mirkin, S. J. Lippard, *J. Am. Chem. Soc.* **2009**, *131*, 14652–14653; b) X.-Q. Zhang, X. Xu, R. Lam, D. Giljohann, D. Ho, C. A. Mirkin, *ACS Nano* **2011**, *5*, 6962–6970.

[11] a)H. Meng, M. Liong, T. Xia, Z. Li, Z. Ji, J. I. Zink, A. E. Nel, *ACS Nano* **2010**, *4*, 4539–4550; b) H. Meng, M. Xue, T. Xia, Y.-L. Zhao, F. Tamanoi, J. F. Stoddart, J. I. Zink, A. E. Nel, *J. Am. Chem. Soc.* **2010**, *132*, 12690–12697.

[12] D. A. Laber, V. R. Sharma, L. Bhupalam, B. Taft, F. J. Hendler, K. M. Barnhart, *J. Clin. Oncol.* **2005**, *23*, 3064.

[13] P. J. Bates, J. B. Kahlon, S. D. Thomas, J. O. Trent, D. M. Miller, *J. Biol. Chem.* **1999**, *274*, 26369–26377.

[14] a) M. Srivastava, H. B. Pollard, *FASEB J.* **1999**, *13*, 1911–1922; b) S. Soundararajan, W. Chen, E. K. Spicer, N. Courtenay-Luck, D. J. Fernandes, *Cancer Res.* **2008**, *68*, 2358–2365; c) Z. Cao, R. Tong, A. Mishra, W. Xu, G. C. L. Wong, J. Cheng, Y. Lu, *Angew. Chem. Int. Ed.* **2009**, *48*, 6494–6498.

[15] D. A. Giljohann, D. S. Seferos, P. C. Patel, J. E. Mill-stone, N. L. Rosi, C. A. Mirkin, **2007**, 7, 3818–3821.

[16] a) J. Liu, Y. Lu, *J. Am. Chem. Soc.* **2003**, *125*, 6642–6643; b) J. Liu, Y. Lu, *J. Am. Chem. Soc.* **2007**, *129*, 8634–8643; c) J. Liu, Y. Lu, *Nat. Protoc.* **2006**, *1*, 246–252; d) J. H. Lee, Z. Wang, J. Liu, Y. Lu, *J. Am. Chem. Soc.* **2008**, *130*, 14217–14226.